J. Fluid Mech. (1989), *vol.* 202, *pp.* 97–115
Printed in Great Britain

Numerical experiments in forced stably stratified turbulence

By JACKSON R. HERRING† AND OLIVIER MÉTAIS†‡
† National Center for Atmospheric Research, PO Box 3000, Boulder, CO 80307, USA
‡ Institut de Mécanique de Grenoble, Domaine Universitaire, BP 53X, 38041 Grenoble Cedex, France

(Received 4 May 1987 and in revised form 30 October 1988)

We present results of numerical simulations of stably stratified, randomly forced turbulence. The selection of forcing and damping are designed to give insight into the question of whether cascade of energy to large scales is possible for strongly stratified three-dimensional turbulence in a manner similar to two-dimensional turbulence. We consider narrow-band wavenumber forcing, whose angular distribution ranges from two-dimensional to three-dimensional isotropic. Our principal results are as follows; for two-dimensional forcing, and for sufficiently small Froude number, the statistically steady state is characterized by a weakly inverse-cascading horizontal-velocity variance field. The vertical variability of the horizontal-velocity field is pronounced, but seems to approach a limit independent of the Brunt–Väisälä frequency N, as $N \to \infty$. If, on the other hand, the Froude number exceeds a critical value, the vertical variability is weak, and the statistics of the scales larger than the forcing scale is near that predicted by inviscid equipartitioning. For all forcing functions considered the vertical motion and temperature field (w, T), centred at smaller scales, are more three-dimensionally isotropic, with no large-scale organization. At large N, (small Froude number) the w-field scales as $1/N$, with horizontal motion field nearly independent of N. Furthermore, at large N and for horizontal forcing, the horizontal motion field is consistent with the condition that a substantial fraction of the total dissipation is attributable to an effective drag acting upon all horizontal scales of motion, which in turn flattens the slope of the energy spectrum in the inverse-cascade range, and increases it in the enstrophy-cascade range.

1. Introduction

The Earth's mesoscale variability (in the range 10 to 1000 km) shows as horizontal-scale distribution ($k^{-\frac{5}{3}}$), whose physics seems to be a combination of strongly stable turbulence and wave motion. Gage (1979) proposed that the observed horizontal variability may be explained as an inverse-cascading two-dimensional turbulence whose physics is similar to that deduced by Kraichnan (1967) for strictly two-dimensional turbulence. In later papers (see e.g. Gage & Nastrom, 1986 for a review) they generalized the discussion to include quasi-geostrophic turbulence such as described by Charney (1971). Lilly (1983) subsequently argued that strong stratification alone implies a dominantly two-dimensional motion. The argument relied on the earlier scaling analysis of Riley, Metcalfe & Weissman (1981). The energy source is at small scales in the range of large-scale thunderstorm activity. An inverse cascade then operates to distribute the energy to progressively larger scales.

We should stress that the motion here envisioned is not two-dimensional; its horizontal components (u, v) have vertical variability which is dynamically determined through dissipative mechanisms, which may involve breaking waves in patches of sufficiently low Richardson number. In addition an effective radiation damping of the wave component should also be introduced in order to properly represent the effects of waves exiting from the region of study. At the large-scale end of this region (1000 km) the effects of rotation must undoubtedly play a significant role, and stratified turbulence merges with a Charney-type (1971) quasi-geostrophic turbulence.

On the other hand, Van Zandt (1982) has argued that the observed data may be entirely explained by gravity waves. Van Zandt finds the atmospheric data consistent with an atmospheric adaptation of the oceanographic Garrett–Munk (1979) internal-wave spectrum. Of vital importance in distinguishing between these various proposals is the vertical variability of both the horizontal motion field and the wave field.

In an effort to understand some of these issues, we examine here, via numerical simulations, strongly stratified turbulence. We focus on homogeneous flows, utilizing a spectral code of resolution $64 \times 64 \times 64$ to resolve the velocity and temperature fields. Additionally, constant fluid properties are assumed. We also remark that although the motivation for the present investigation derives from the meteorological problem noted above, the problem examined here is of a purely fluid dynamical character.

The equations of motion to be investigated are the Boussinesq set:

$$\left(\frac{\partial}{\partial t}+\nu(\nabla^2)\right)\boldsymbol{u} = -\nabla p - \boldsymbol{u}\cdot\nabla\boldsymbol{u} + \hat{\boldsymbol{g}}\alpha T + \boldsymbol{F}, \tag{1}$$

$$\left(\frac{\partial}{\partial t}+\kappa(\nabla^2)\right)T = -\beta w - \boldsymbol{u}\cdot\nabla T + F_T \tag{2}$$

and

$$\nabla\cdot\boldsymbol{u} = 0. \tag{3}$$

Here, $\beta(>0)$ is the constant horizontally averaged temperature gradient, α is the fluid expansivity, and $\hat{\boldsymbol{g}}$ is the unit vertical vector. The (constant) Brunt–Väisälä frequency is $N = (-\alpha\beta)^{\frac{1}{2}}$. The quantities $\nu(\nabla^2)$ or $K(\nabla^2)$ represent hyperviscosity (or conductivity), whose form is $(\nu_0, K_0)\nabla^2 + (\nu_2, K_2)\nabla^4$. Terms $(\nu_2 K_2)$ are needed here to damp small scales, preventing possible accumulation of energy (or temperature variance) at the smallest resolvable scales. We are interested in homogeneous flows for which the collocation basis set

$$\exp(2\pi i n x/L), \quad n = \pm(0, 1, 2, \ldots)$$

suffices along each of the Cartesian axes (x, y, z). Here, L is the periodic box length, which we set to unity for simplicity. We denote by the vector $\boldsymbol{k}$ the triplet-collection $\pm 2\pi(0, 1, 2, \ldots)/L$, and take z to be the vertical. To solve (1)–(3), we use collocation with the above basis set. The time stepping is by the leap-frog scheme, stabilized by periodic averaging with Crank–Nicholson stabilization of large wavenumbers. This procedure has had ample discussion (Orszag & Patterson 1972; Riley *et al.* 1981; Curry *et al.* 1984).

The present problem has both wave and turbulent components. For linear problems, it is clear how to distinguish between these degrees of freedom: take one component 'along' the gravity wave and the other orthogonal to the first component.

If incompressibility is included, these suffice to represent $\boldsymbol{u}(x,t)$. These components, denoted here as (ϕ_1, ϕ_2), are conveniently represented in wavenumber space by

$$\phi_1(\boldsymbol{k}) = [(\boldsymbol{k}\times\hat{\boldsymbol{g}})\cdot\boldsymbol{u}]/|(\boldsymbol{k}\times\hat{\boldsymbol{g}})| \tag{4}$$

and

$$\phi_2(\boldsymbol{k}) = [(\boldsymbol{k}\times(\boldsymbol{k}\times\hat{\boldsymbol{g}})\cdot\boldsymbol{u}]/|\boldsymbol{k}\times(\boldsymbol{k}\times\hat{\boldsymbol{g}})|. \tag{5}$$

In terms of these we may write $\boldsymbol{u}(\boldsymbol{k},t)$ as

$$\boldsymbol{u}(\boldsymbol{k},t) = [(\boldsymbol{k}\times\hat{\boldsymbol{g}})/|\boldsymbol{k}\times\hat{\boldsymbol{g}}|]\,\phi_1 + [\boldsymbol{k}\times(\boldsymbol{k}\times\hat{\boldsymbol{g}})]/|\boldsymbol{k}\times(\boldsymbol{k}\times\hat{\boldsymbol{g}})|\,\phi_2. \tag{6}$$

Associated with $\phi_1(\boldsymbol{k})$, $\phi_2(\boldsymbol{k})$ are their intensities, $\Phi_1(\boldsymbol{k})$, $\Phi_2(\boldsymbol{k})$:

$$\Phi_i(\boldsymbol{k}) \equiv \langle \phi_i^*(\boldsymbol{k})\,\phi_i(\boldsymbol{k})\rangle, \quad i = 1,2. \tag{7a}$$

Here, the angular brackets denote an ensemble average. We also introduce the potential energy spectrum:

$$P(\boldsymbol{k}) \equiv \tfrac{1}{2}\langle T^*(\boldsymbol{k})\,T(\boldsymbol{k})\rangle/\beta. \tag{7b}$$

Following an existing terminology, we shall call ϕ_1 the 'turbulence' (or 'vortical' mode) and ϕ_2 the wave mode, despite the fact that for strongly nonlinear flows the identification of ϕ_2 with the waves and ϕ_1 with the 'turbulence' is not justified. The components (ϕ_1, ϕ_2) were introduced into the study of internal waves by Riley *et al.* (1981) and Lilly (1983) as a convenient description of waves and turbulence. They also serve as an economical description of axisymmetric turbulence (Craya 1958; Herring 1974) without waves.

To set the stage for the numerical study that follows, we sketch for a simple problem how it is consistent that horizontal motion may dominate (as $N\to\infty$) by perturbatively estimating – in this limit – the intensity, $\Phi_2 \equiv \langle \phi_2^*(\boldsymbol{k},t)\,\phi_2(\boldsymbol{k},t)\rangle$. For this purpose, it is convenient to use the resolution (4), (5), and (6) in the Navier–Stokes equations. In the latter, we shall put $F_3 = F_T = 0$, and take (F_1, F_2) two-dimensionally isotropic. We shall, moreover, take (F_1, F_2) to be centred in a narrow band of wavenumbers at small scales, so that the forcing does not interfere with any possible inverse cascade. Under these assumptions, the activation source for $\phi_2(\boldsymbol{k})$ stems from the nonlinearity (ϕ_1, ϕ_1) in (1) and (2). Eliminating $\partial_t T$ from the set of equations for $(\partial_t\phi_2, \partial_t T)$ then gives

$$(\partial_t^2 + N^2\sin^2\theta)\,\phi_2(\boldsymbol{k},t) = \partial_t \sum_{\boldsymbol{k}=\boldsymbol{p}+\boldsymbol{q}} E(\boldsymbol{k},\boldsymbol{p},\boldsymbol{q})\,\phi_1(\boldsymbol{p})\,\phi_1(\boldsymbol{q}) + \ldots. \tag{8}$$

Here, $E(\boldsymbol{k},\boldsymbol{p},\boldsymbol{q}) \equiv iq\boldsymbol{e}_2(\boldsymbol{k})\cdot(\boldsymbol{e}_1(\boldsymbol{p})\times\boldsymbol{e}_2(\boldsymbol{q}))$, $\boldsymbol{e}_1$ and $\boldsymbol{e}_2$ are the vector coefficients of ϕ_1 and ϕ_2 in (6), and $\cos\theta = \boldsymbol{k}\cdot\hat{\boldsymbol{g}}/k$. That $\Phi_2 \sim N^{-2}$ follows from (8) if the timescales of its right-hand side are of order N^{-1}. Note that the right-hand side of (8) pertains to the vertical (and temporal) variability of ϕ_1; it is zero for static ϕ_1, or for a strictly two-dimensional flow.

Although the above discussion suggests a dominance of stratified turbulence at large N, all we may really conclude is that the initial rate of growth of the wave component is $1/N$: the eventual $t\to\infty$ state (far from the region of forcing) could be equipartitioning among independent degrees of freedom (the three velocity components and the potential temperature). Indeed, the application of statistical mechanical reasoning to the inviscid, unforced subset of (1)–(3) would lead to this conclusion. What may save the argument for the dominance of stratified turbulence as $N\to\infty$ is that dissipation may affect the stratified component differently than the

wave component. We note, in this connection, that if the stratified component has a strong inverse transfer to large scales, its energy will be centred at small k and hence suffer relatively little dissipation, whereas the wave component, having no inverse transfer tendency, may be subject to stronger dissipation.

We have suggested a two-dimensional dynamics for the regime $N \to \infty$ (through (8)), but the discussion is clearly incomplete since the statistics of the z-dependence of ϕ_1 is undetermined. This question is also related to the vertical stability of the flow (in the sense of Richardson), and the constraint that its steady-state dissipation equals the energy input by $\boldsymbol{F}$. We are as yet unable to see how an extension of the perturbation theory sketched above determines, in the statistically steady state, quantities like $\langle \boldsymbol{u}(\boldsymbol{x}, z, t)\, \boldsymbol{u}(\boldsymbol{x}, z', t) \rangle$ as functions of forcing. For this reason, and because the vertical variability is vital in any quantitative discussion of stratified turbulence, we focus on numerical experiments in which the forcing is strictly two-dimensional, so that any vertical variability is wholly attributable to nonlinear dynamics, and not to arbitrary forcing.

In the atmosphere, the wave component exits the layer studied at the stratosphere, where wave breaking associated with a non-constant density gradient occurs. This provides an additional damping for the wave component. D. K. Lilly (private communication, 1985) has made a proposal to estimate this effect, within the confines of a homogeneous calculation. In the present study, we shall subordinate this important empirical aspect of the problem in order to first stress the basic fluid mechanics. For sufficiently strong stratification such damping may be unnecessary, since the wave component is in this case small.

2. Some numerical results

2.1. *Statement of problem to be studied*

In order to have a reference case to which to compare our results, we consider first a two-dimensional flow randomly forced at small scale, for which we may demonstrate an inverse-cascade range at scales larger than the forcing wavenumber. Having found a suitable (two dimensional) forcing and dissipation, we then introduce a small three-dimensionalized perturbation, and allow the system to evolve to its stationary states. This two-dimensional reference problem has special features which should be noted. First, the total energy eventually increases without bound, if the lowest available wavenumber $k_{\mathrm{L}} = 0$ (Kraichnan 1967). For non-zero k_{L}, which is our case, the flow stabilizes at a finite energy, but eventually may collapse into a near non-turbulent circulation with little transfer to large scales. Any useful analogy between stratified flow and two-dimensional turbulence can hold only during the inverse-cascading phase, prior to the collapse. As it turns out, and our numerical calculations support this picture, the rate at which the total kinetic energy increases is slow compared with the rate at which scales in the range $(0.1k_{\mathrm{f}} \leqslant k \leqslant k_{\mathrm{f}})$ assume their cascade-equilibrium shape (i.e. $k^{-\frac{5}{3}}$). (Here, k_{f} is the forcing wavenumber.) Hence we define our reference problem as the two-dimensional forced problem during that time span for which the inverse cascade is vigorous, and during which the energy slowly increases.

For the present set of runs, the flow is forced by a two-dimensional Markov forcing of the (u, v)-fields on a wavenumber band

$$(k_{\mathrm{B}} = 10 < k < 12 = k_{\mathrm{T}}).$$

	I	N	ν	γ	k_f	dt
Run 1	1	—	0.005	16	11	0.000625
Run 2	1	20π	0.005	16	11	0.000625
Run 3	1	40π	0.005	16	11	0.000625
Run 4	1	80π	0.005	16	11	0.0003125

TABLE 1. Parameters of two-dimensionally forced runs $\eta = 5$, $I = 1$, $\kappa = \nu$ (see (9))

It is non-zero only for the vertical wavenumber zero. We define $k_f = \frac{1}{2}[k_B + k_T]/2$ to be the centroid of the forcing wavenumber band. The forcing function $F_i(t)$ is Markov (in time), with no correlation between wavenumber vectors. As applied to each wave component of the field $\boldsymbol{u}$, $\boldsymbol{F}$ satisfies

$$\langle F_i(t) F_j(t') \rangle = I(k) (e_1^i e_1^j) \exp(-\eta|t-t'|) \delta(k_z). \tag{9}$$

The angular brackets represent an ensemble (or time) average. We do not force the temperature field. $I(k)$ is quadratically distributed in k, vanishing at k_B and k_T. Values of the integral I and η for the present runs are given in table 1 along with the 'hyperviscosity' $\nu(k)$ and hyperconductivity $\kappa(k)$, written here in the form

$$\nu(k) = \nu_0 k^2 (1 + \gamma(k/k_f)^2), \quad \kappa(k) = \nu(k). \tag{10}$$

Also given in table 1 are the forcing wave number k_f, the time step, dt, and γ, an adjustable constant entering (10). As noted above, the use of a hyperviscosity is necessary in order to attenuate spectra at large k, so that high-wavenumber truncation errors (near $k = 32$) are small. We have further set k_f at the rather small value (11) in order to keep the large-scale dynamics as free as possible of collocation-aliasing errors.

After describing the two-dimensional solution, we investigate in the following sections the behaviour of the randomly forced system if submitted to a small initial temperature perturbation. We then explore the nature of the stationary state as the Brunt-Väisälä frequency varies.

2.2. *Statistical features of the flow: energies, variances, spectra, and distribution functions*

Figure 1 (*a*) shows the curve of $[\langle u^2 \rangle, \langle v^2 \rangle](t)$ for Run 1, a strictly two-dimensional flow with no vertical motion or temperature fluctuations. After the initial transient phase, these grow slowly and approximately exponentially. The spectrum

$$E_\perp(k, t) = \tfrac{1}{2}[\langle |u|^2 \rangle (k) + \langle |v|^2 \rangle (k)] \equiv \Phi_1(\boldsymbol{k}) \tag{11}$$

is shown in figure 1 (*b*) for $t = 0.938$. The inverse cascade for $k < k_f$ is clearly visible, although the resolution here (64^3) is small by contemporary two-dimensional standards ($\geqslant 128^2$). Nevertheless, the slope of the spectrum for $k < k_f$ is close to $k^{-\frac{5}{3}}$. Beyond $t = 1$, energy begins to accumulate significantly at the largest available scale, $[(2\pi/k_L), k_L = 1]$, and a time-step smaller than that in table 1 must be used to prevent the system from blowing up.

We consider next, in Runs 2 to 4, what happens if a small random (Gaussian)

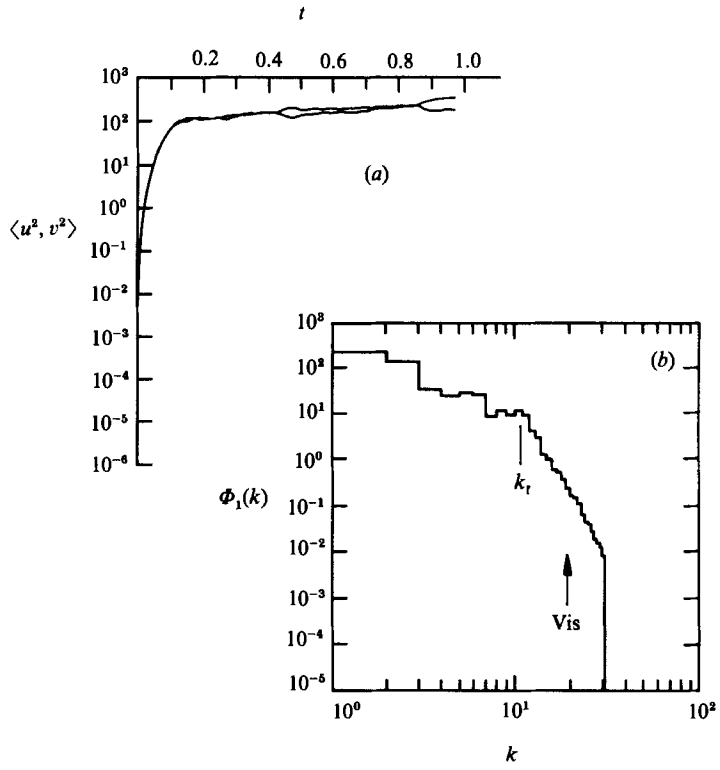

FIGURE 1. (*a*) Kinetic energy as a function time t for Run 1 (see table 1), showing $\langle u^2(t)\rangle$, and $\langle v^2(t)\rangle$, where angular brackets denote volume average. The system is forced randomly, but only two-dimensional modes are activated (i.e. $F \neq 0$ only if $k_z = 0$: $F_w(t) = F_T(t) = 0$). (*b*) Two-dimensional energy spectrum $E_\perp(k,t)$ (see (11)) for Run 1 at $t = 0.938$. The histogram shows the totals of $\frac{1}{2}[u^2(k,t)+v^2(k,t)]$ for the wavenumber bins whose magnitude limits are $(1,2,\ldots,31)$. The arrow marks the beginning of the range of strong viscous dissipation (i.e. $\nu(k) > [k^3E(k)]^{\frac{1}{2}}$, see (10)).

temperature perturbation is introduced at $t = 0$ and N is progressively increased, as indicated in table 1. The perturbation spectrum is

$$\langle T(\boldsymbol{k})\, T(-\boldsymbol{k})\rangle = Ck^4 \exp\left(-2(k/k_0)^2\right), \tag{12}$$

where $C = 1\times10^{-5}$, and $k_0 = 4.760$. Figure 2 shows $\frac{1}{2}(\langle u^2\rangle(t), \langle v^2\rangle(t))$, the vertical velocity field variance

$$E_w(t) = \tfrac{1}{2}\langle w^2\rangle, \tag{13}$$

and potential energy

$$P(t) = \tfrac{1}{2}\langle T^2\rangle/\beta \tag{14}$$

for the range of N ($\alpha\beta = N^2$) given in table 1. We note the initial exponential growth of $E_w(t)$ and $P(t)$. The rate shows no discernible dependence on N. Wave activity is manifest only during the initial, linear phase. Apparently (w, T) evolve as a linear wave for a short time before the shear in the horizontal motion field induces an instability which returns the system toward isotropy. The 'return to isotropy rate' during the initial phase is well represented by the empirical formula

$$\frac{\mathrm{d}[\ln(E_w(t)), \ln(P(t))]}{\mathrm{d}t} \approx -0.657(\Phi_1^{\mathrm{tot}})^{\frac{1}{3}} k_f. \tag{15}$$

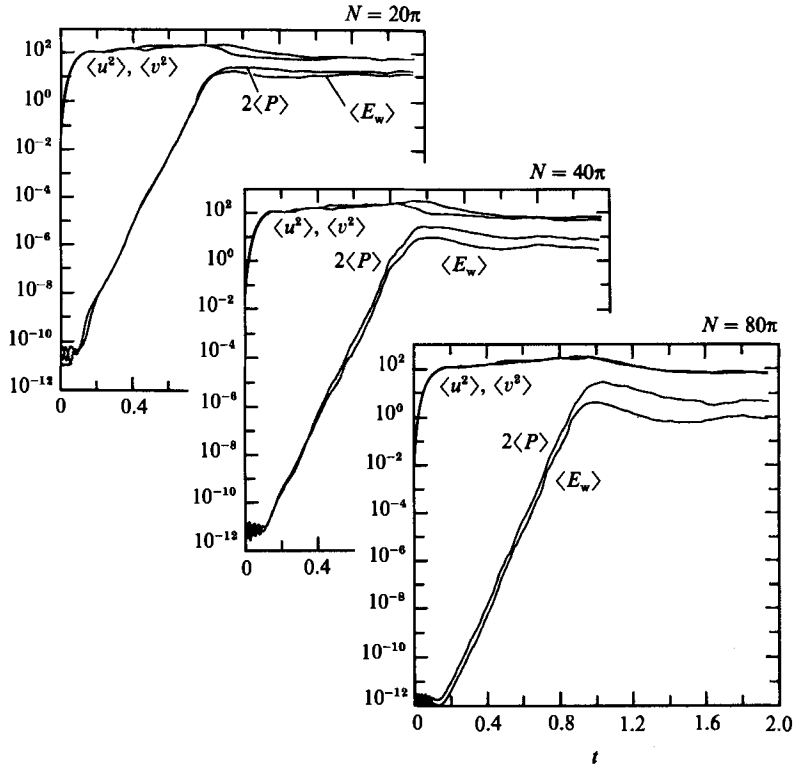

FIGURE 2. $\langle u^2\rangle(t)$, $\langle v^2\rangle(t)$, vertical variance energy $E_w(t)$, and total potential energy $P(t)$, for Run 2. Temperature at $t = 0$ is as specified by (12), and $w(k, 0) = 0$ for $N = (20\pi, 40\pi, 80\pi)$. Notice the slow exponential increase of $E_\perp(t)$ until $E_w(t)$ and $P(t)$ near their saturation level, after which the system approaches statistical equilibrium.

Here, Φ_1^{tot} is the total (wave-vector sum) of the $\Phi_1(\boldsymbol{k})$ field (see (7 *a*) and (4)). The equilibrium value of E_w is in rough accord with the scaling arguments of equation (8) ($E_w \sim N^{-2}$). $E_w(t)$ is smaller than P, a result of the strong vertical variability that ensues at large N.

Spectra for Φ_1, Φ_2, and P are shown in figures 3–6. We show here isotropically accumulated spectra (figure 3); vertical wavenumber (k_z) spectra (figure 5); and horizontal wavenumber ($K_\perp$) spectra (figure 6) for the three values of $N = (20\pi, 40\pi, 80\pi)$, respectively. Figure 4 shows $R_2(k)$, the intensity of the second spherical harmonic of Φ_1, Φ_2, and $P(\boldsymbol{k}, t)$. These are defined by

$$R_2(k) = \int_{-1}^{1} \mathrm{d}\mu P_2(\mu)\, \Psi(\boldsymbol{k})/\Psi(k), \quad \mu = k_z/k, \tag{16}$$

where $P_n(\mu)$ is the nth Legendre polynomial, and Ψ stands for (Φ_1, Φ_2 or P).

Examining first figure 3, we see little evidence of inverse cascade at $N = 20\pi$ (the solid lines). In fact, the spectrum below k_f is not too dissimilar from inviscid equilibrium, $\sim k^2$, except at the lowest available $k-$bin. For $N = 20\pi$ the R_2-harmonic amplitude as shown in figure 4 (see (16)) is mildly two-dimensional ($R_2 \leqslant 0$) for $\Phi_1(\boldsymbol{k})$, with moderate vertically variability for Φ_2 and P. (For isotropic fields $R_2 = 0$, and for strict two-dimensionality (no k_z dependence) $R_2 = -\frac{2}{5}$.) At the same time, figure 3 shows that for $N = 20\pi$, Φ_2 and P remain in close equipartition over the

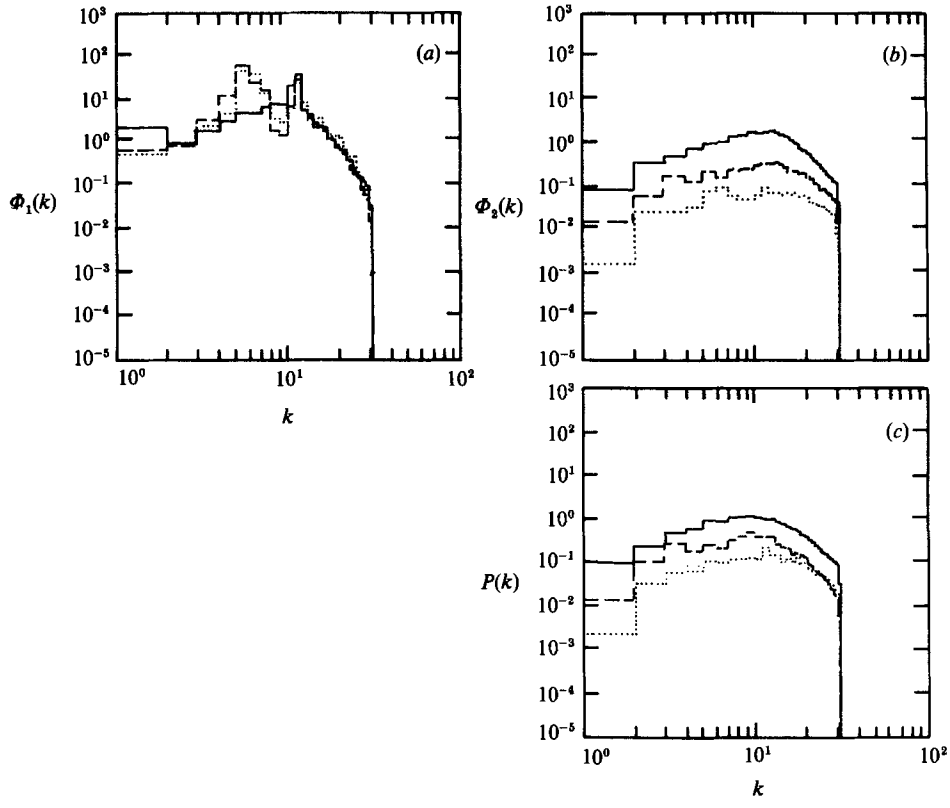

FIGURE 3. Angular average energy spectra: (a) $\Phi_1(k,t)$; (b) $\Phi_2(k,t)$; (c) $P(k,t)$. Here $t = 3.90$; ——, $N = 20\pi$; – – – –, 40π; · · · · ·, 80π.

full spectral range (as we shall shortly see, this equipartition holds only for $N \lesssim 20\pi$). As N increases, a spectral bulge develops near $k \approx 5$, the R_2-spectra for Φ_2 becomes saturated at extreme vertical variability ($R_2 = +1$) at roughly $k = 5$. An examination of the higher P_m harmonics shows that these, too, are saturated, which implies an angular distribution close to $\delta(|\mu|-1)$: thus the variability in the range ($4 \leqslant k \leqslant 8$) is almost entirely k_z. Note that $\Phi_2(k)$ and $P(k)$ spectra both decrease in accordance with the comments following (8).

We turn now to the vertical wavenumber spectra (figure 5). We note a striking increase of vertical instability in the region ($k_z > 5$) as N increases beyond 20π. This abrupt increase in variability suggests that a stability threshold is crossed. Once crossed, little change in the spectrum $\Phi_1(k_z)$ (in either shape or intensity) is noted. These Φ_1 spectra for $k_z \gtrsim 5$ are not inconsistent with a k_z^{-3} law. However, they do not scale as $N^2 k_z^{-3}$ (as would be the case were the energy spectrum determined exclusively by N), but become independent of N, if Runs 3 and 4 indicate the trend as $N \to \infty$. Note that $P(k_z)$ for the two larger values of N are nearly equal (for $k_z < 11$), despite the fact, as noted above, that $P(k)$ progressively decreases with increasing N. Neither $P(k_z)$ nor $\Phi_2(k_z)$ show power-law behaviour at large k_z, although the range of scales considered here ($0 < k_z < 31$) is probably too small to discuss this issue adequately.

An interesting but unanswered question here is why the $\Phi_1(k_z)$-spectrum drops rapidly for $k_z \leqslant k_z^0 = 5$. This value of k_z sets the number of vertical layers, whose thickness $\Lambda \approx (1/k_z^0)$ could possibly be affected by the presence of the low-

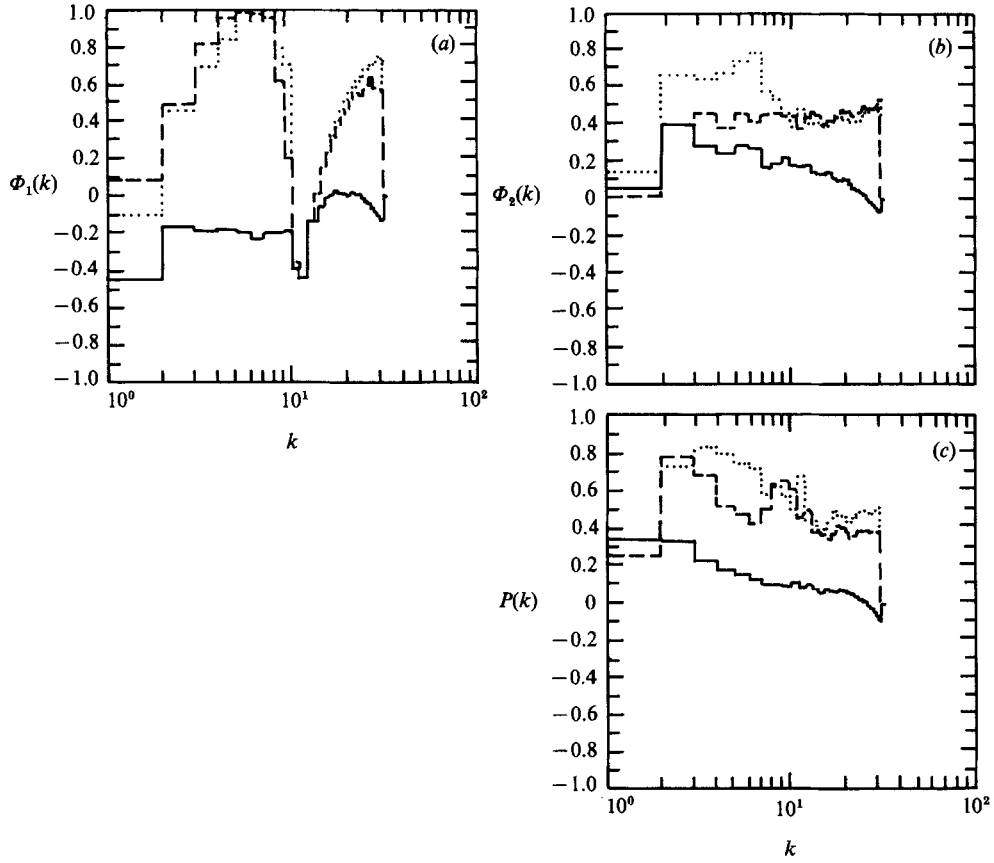

FIGURE 4. Second angular harmonics R_2 (see (16)) for fields $\Phi_1(k)$, $\Phi_2(k)$, and $P(k)$, and ——, $N = 20\pi$; – – – –, 40π; · · · · ·, 80π.

wavenumber cutoff, k_L, but is more likely determined by dynamical considerations. The fact that $\Phi_1(k_z)$ has a non-exponential slope at small $k_z(k_z^{-3}?)$, followed by a dissipation range (see figure 5*a*) suggests that Λ is not simply determined by purely dissipative effects. Fernando (1988) has proposed, for freely evolving turbulence, that Λ is several Ozmidov (1965) lengthscales. However, we note that for the present forced problems the Ozmidov scale $(2\pi/k_O, k_O \equiv (N^3/\epsilon)^{\frac{1}{2}})$ is much smaller than the layer thickness ($k_O \approx 80$, for $N = 80\pi$). Moreover, Λ seems insensitive to N, according to figure 5. Perhaps more plausibly, in our case Λ is determined by the condition that the frictional effect of the layering balances the input of energy by random forcing.

The stability issue mentioned above is presumably related to a suitably defined Richardson number for the flow. For the present problem, the definition

$$Ri = N^2/\langle(\partial u/\partial z)^2\rangle \tag{17}$$

seems plausible. It is also useful to have a dynamically defined Froude number, which we take to be

$$Fr = \langle u^2\rangle^{\frac{1}{2}}/LN, \tag{18a}$$

where

$$L = \int_{-\infty}^{\infty} \mathrm{d}\zeta\langle\phi_1(x, y, z+\zeta)\,\phi_1(x, y, z)\rangle/\langle\phi_1^2\rangle \tag{18b}$$

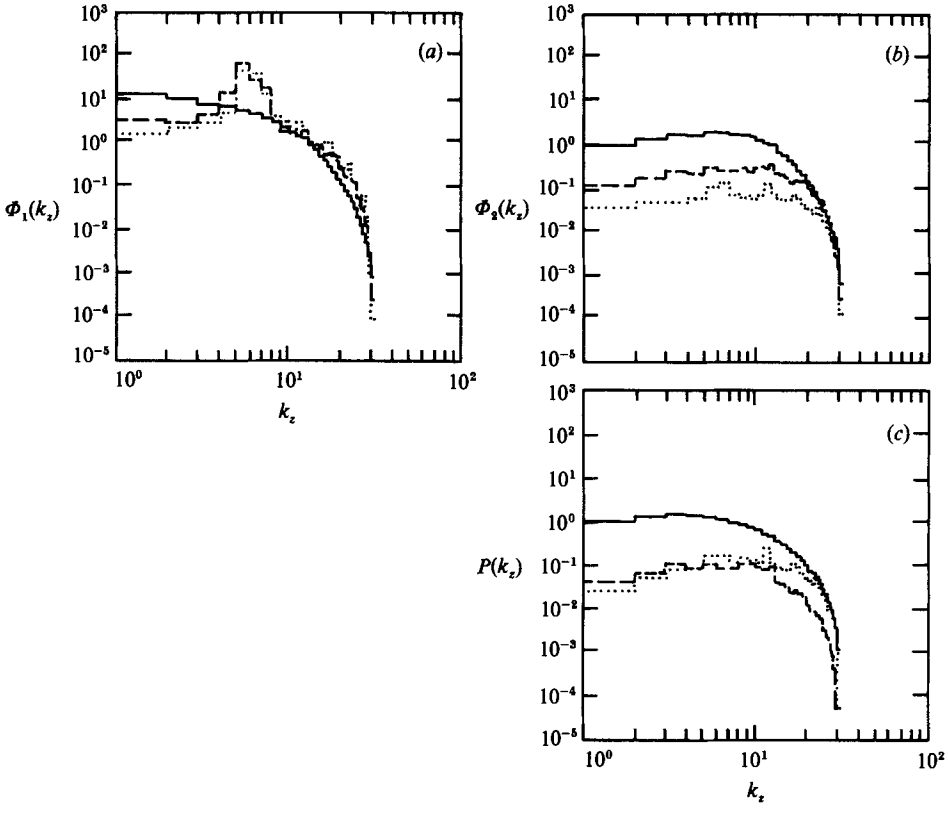

FIGURE 5. Vertical wavenumber spectra for Run 2: (*a*) $\Phi_1(k_z,t)$; (*b*) $\Phi_2(k_z,t)$; (*c*) $P(k_z,t)$ at $t = 3.90$. ——, $N = 20\pi$; – – – –, 40π; · · · · ·, 80π.

Run	$Ri^{\frac{1}{2}}$	Fr
2	1.02	0.387
3	2.02	0.884
4	4.06	0.197

TABLE 2. Froude and Richardson numbers (see (18) and (17))

is the vertical integral scale for ϕ_1. Note that (17) and (18*a*, *b*) differ in that Ri is a microscale quantity, whereas Fr is a macroscale quantity. Table 2 lists Ri and Fr for the three runs discussed here. The variation of Ri here is consistent with the idea that $N = 20\pi$ is unstable with respect to vertical overturning, whereas $N = (40\pi, 80\pi)$ are not. The value of Fr for Run 3 is anomalously large: the value of L entering its definition (18*b*) has abruptly become smaller because the flow has made a transition to a layered state on going from Run 2 to Run 3.

We consider in figure 6 two-dimensional spectra, functions of $K_\perp$,

$$K_\perp = (k_x^2 + k_y^2)^{\frac{1}{2}}.$$

The spectrum $\Phi(K_\perp)$ is the quantity to which to compare the two-dimensional results shown in figure 1(*b*). We note a slight inverse cascade for $\Phi_1(K_\perp)$ for $N = (40\pi, 80\pi)$. The peaks in these spectra at k_f are, of course, attributable to the forcing in the band of wavenumbers centred at k_f. However, unlike the two-dimensional flow, which has

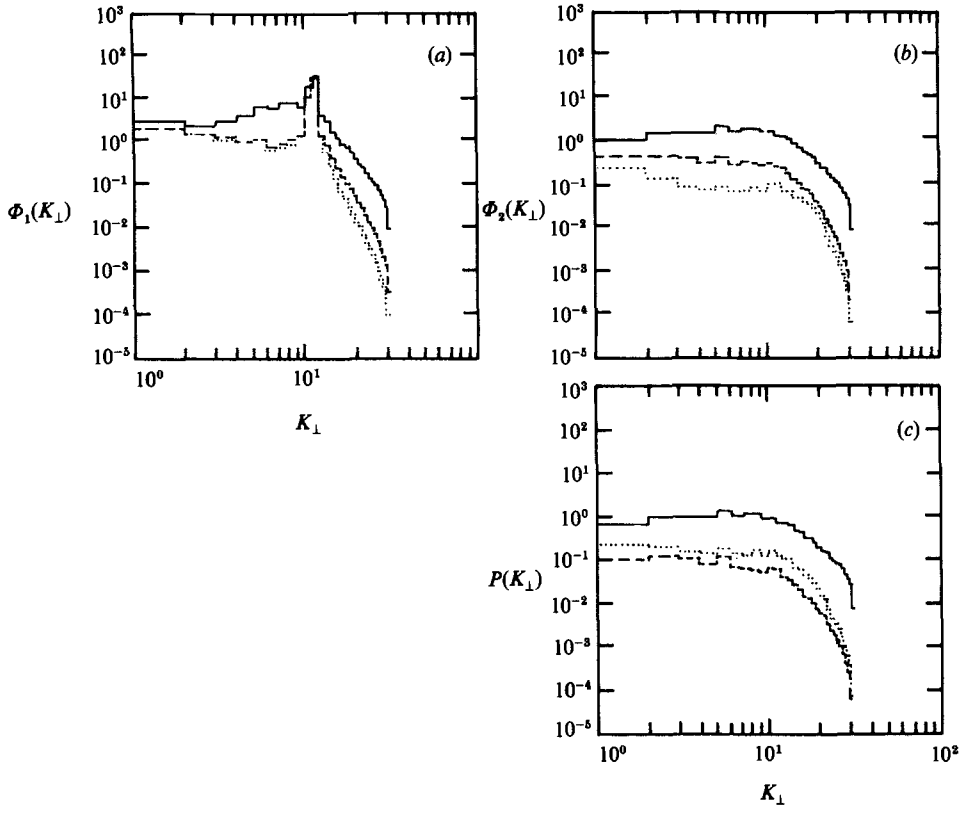

FIGURE 6. Horizontal ($K_\perp = (k_x^2 + k_y^2)^{\frac{1}{2}}$) wavenumber spectra for (*a*) $\Phi_1(K_\perp, t)$; (*b*) $\Phi_2(K_\perp, t)$; (*c*) $P(K_\perp, t)$. Here $t = 3.90$; ——, $N = 20\pi$; – – – –, 40π; · · · · ·, 80π.

a hearty inverse cascade, as shown in figure 1(*b*) (for the same forcing and dissipation), the present system is unable to transfer effectively our of the forcing region. Again, in the wavenumber range $k < k_f$ the Φ_1 spectrum seems to saturate, with little significant change on passing from Run 3 to Run 4, as N doubles. For $K_\perp > K_{\perp f}$, however, the spectral slope increases with increasing N.

It is of interest to examine the various energy fluxes into Φ_1, Φ_2, and $\langle |T|^2 \rangle$. This is conveniently done by introducing the transfer function, $\mathscr{T}(\boldsymbol{k}, t)$, defined such that

$$\frac{\partial \Phi_i(\boldsymbol{k}, t)}{\partial t} \equiv \mathscr{T}_i(\boldsymbol{k}, t) - 2\nu(k^2)\, \Phi_i(\boldsymbol{k}, t) + \langle F_i(\boldsymbol{k}, t)\, \Phi_i^*(\boldsymbol{k}, t) + F_i^*(\boldsymbol{k}, t)\, \Phi_i(\boldsymbol{k}, t) \rangle. \tag{19}$$

Here, as before angular brackets stand for an ensemble average. In practice, we replace the ensemble average with a wavenumber-band average over a group of statistically equivalent $\boldsymbol{k}$: in our case, an average over the direction of axisymmetry, and a shell average over discrete radial wavenumber bins. The first of these, applied to (19) suffices to make the time derivative zero if the flow is statistically stationary. We may further analyse $\mathscr{T}_i$ into contributions from vortical–vortical (vv), vortical–wave (vw), and wave–wave (ww) contributions. (Recall that by vortical, we mean simply ϕ_1; and by wave ϕ_2.) The $\mathscr{T}(\boldsymbol{k}, t)$ for $\Phi_1(\boldsymbol{K}_\perp, t)$, for example, is

$$\mathscr{T}_{\mathrm{v}}(K_\perp) = \mathscr{T}_{\mathrm{vvv}}(K_\perp) + \mathscr{T}_{\mathrm{vwv}}(K_\perp) + \mathscr{T}_{\mathrm{vww}}(K_\perp), \tag{20}$$

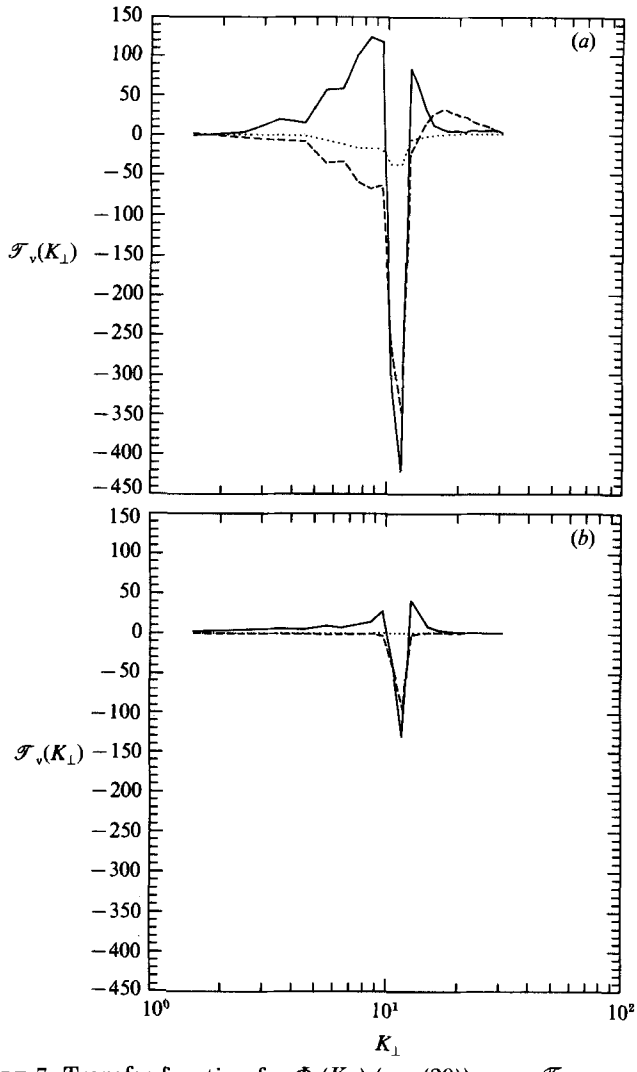

FIGURE 7. Transfer function for $\Phi_1(K_\perp)$ (see (20)): ——$\mathscr{T}_{vvv}$, – – –$\mathscr{T}_{vwv}$, · · · · ·$\mathscr{T}_{vww}$. (*a*) $N = 20\pi$, (*b*) $N = 80\pi$.

where the first subscript tags the vortical mode, and the remaining (vv, wv, or ww) signify the interactions between vortical–vortical, wave–vortical, or wave–wave modes that feed energy into the vortical mode. $\mathscr{T}_v$ is shown in figure 7 for Runs 2 and 4. We note, overall, a dramatic reduction in $\mathscr{T}_v(k)$ on passing from Run 2 ($N = 20\pi$) to Run 4 ($N = 80\pi$). The strictly two-dimensional terms (vvv) for both runs (especially Run 4) resemble a two-dimensional forced energy transfer function. Among terms contributing to $\mathscr{T}_v(K_\perp)$, vww is smallest, and becomes relatively smaller as N increases. On the other hand, vwv (the wave–vortex interactions) drain the stratified turbulence with the same intensity as the vortex–vortex interactions in the forcing-wavenumber region. This is true for both runs, suggesting that near the forcing scale, the wave component cannot be neglected for any N. At small $K_\perp$, there is a significant transfer of energy into $\Phi_1(K_\perp)$, which must be balanced (in the steady state) by viscous effects alone, since all other transfers are small.

Another interesting statistical aspect of the flow is the probability distribution

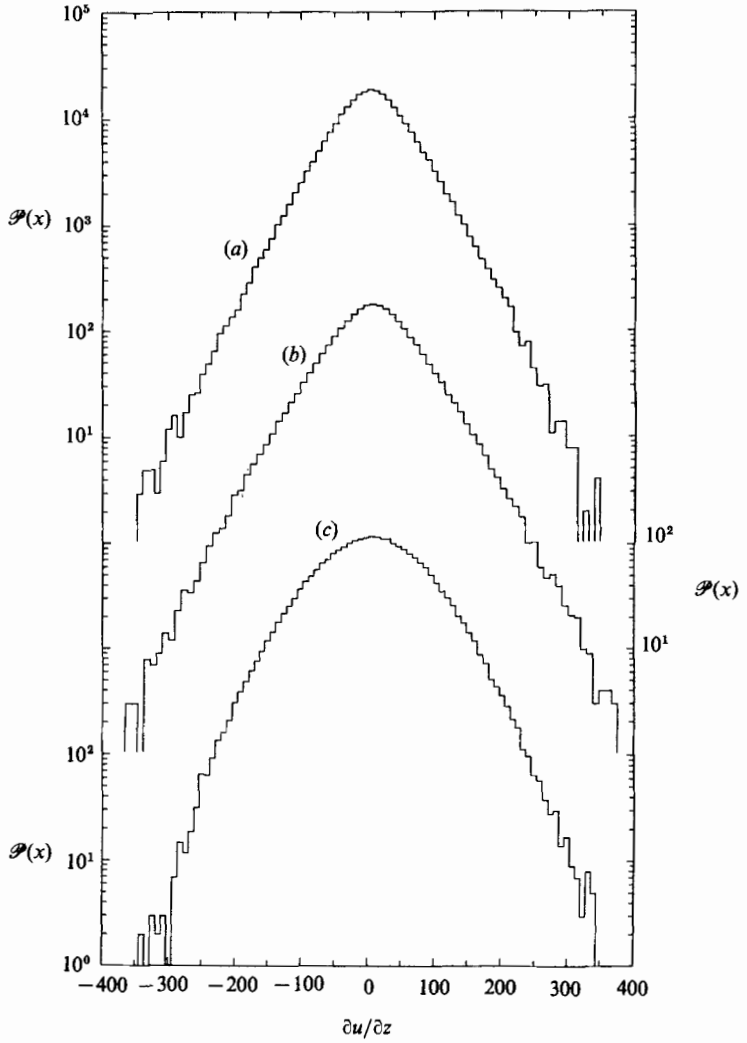

FIGURE 8. Differential distribution function for $x = \partial u/\partial z$ for (*a*) $N = 0$, (*b*) 20π, (*c*) 80π (runs 1, 3, 4).

function, $\mathscr{P}(x)$, that some flow property x (= a velocity derivative, etc.) lies between x and $x+\mathrm{d}x$. We discuss here two such distributions: that for $\partial u/\partial z = x$, and the helicity, $x = \boldsymbol{u}\cdot(\boldsymbol{\nabla}\times\boldsymbol{u})$. The first may aid in assessing the statistical stability of the flow against vertical overturning. We consider first $x = \partial u/\partial z$, as shown in figure 8, for $N = (0, 20\pi, 80\pi)$. As N increases, the cores of these distributions decrease, with a corresponding increase in the wings. An interesting feature here is that, especially for small N, the wings have a significant exponential range (i.e. $\mathscr{P}(x) \sim \exp(-a|x|)$). For $N \to 0$, such an exponential distribution holds over the range $100 \leqslant |x| \leqslant 300$, during which $\mathscr{P}$ decreases by about three orders of magnitude. Similar results have been found in other contexts; for example the shear-flow experiments of Anselmet *et al.* (1984), who find exponential distributions for structure functions, and the quasi-geostrophic turbulence simulations of McWilliams (1989), who observes a similar behaviour for the potential vorticity distribution. Our results here differ from those of McWilliams in that ours do not show an intense central core, as do his. The latter behaviour is an indication of strong intermittency.

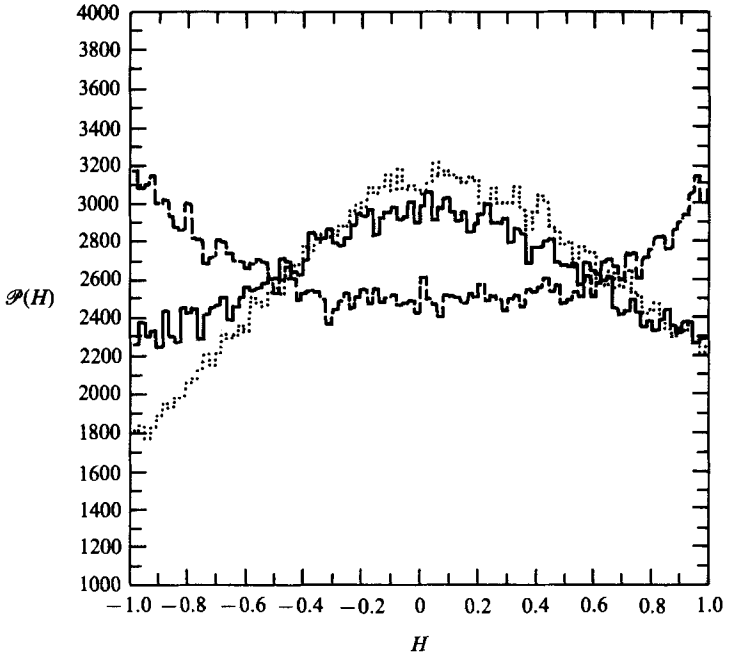

FIGURE 9. Differential distribution function for helicity $H = \boldsymbol{u}\cdot(\boldsymbol{\nabla}\times\boldsymbol{u})$ for $N = 0$ (– – – –); 20π (——); 80π (· · · · ·).

The helicity density is defined as

$$H(\boldsymbol{x},t) = (\boldsymbol{u}(\boldsymbol{x})\cdot(\boldsymbol{\nabla}\times\boldsymbol{u}(\boldsymbol{x})). \tag{21}$$

Its volume integral is an inviscid constant of motion. Several recent numerical and theoretical studies (Kerr 1987; Pelz, Shtilman & Tsinober 1986; Levich & Tsinober 1983) suggest that the Navier–Stokes dynamics is such that regions contain little dissipation. To examine this issue, it is customary to invoke a conditional distribution $\mathscr{P}(\zeta,f)$, defined as the probability that ζ is in $(\zeta,\zeta+\mathrm{d}\zeta)$ on condition that some quantity, for example a locally defined dissipation $\zeta \equiv D(\boldsymbol{x},t) \equiv \frac{1}{2}[\partial u_i/\partial x_j + \partial u_j/\partial x_i]^2$, does not exceed a fraction f of its spacial average value. Pelz *et al.* (1986) chooses $f = 0.001$. Figure 9 shows $\mathscr{P}(\boldsymbol{x}\,|\,f)$ for $N = (0, 20\pi, 80\pi)$, and for $f = 1$. We pick $f = 1$ since there now appears to be a reasonable doubt that strong helicity inhibits dissipation (Kerr 1987). For $N = 0$ (dashed line), $\mathscr{P}(x\,|\,f)$ is somewhat peaked at $|x| = 1$. A sharply peaked distribution would correspond to intrinsic stability of structures for which $\boldsymbol{u}$ parallels $\boldsymbol{\nabla}\times\boldsymbol{u}$. We should remark, in this connection, that $\mathscr{P}(x = \boldsymbol{a}\cdot\boldsymbol{b}/|\boldsymbol{a}|\,|\boldsymbol{b}|) = 1/4\pi$, if $(\boldsymbol{a},\boldsymbol{b})$ are Gaussian, uncorrelated, random three-dimensional vectors. We have further confirmed (numerically) that $\mathscr{P}(x)$ is quite flat if Gaussian (incompressible) $\boldsymbol{u}$ is used. For strong stratification, however, (solid line, $N = 20\pi$; dotted, $N = 80\pi$) we observe the converse: $\boldsymbol{u}$ and $\boldsymbol{\nabla}\times\boldsymbol{u}$ tend to be more nearly orthogonal. We have observed a similar behaviour in thermal convection: in both problems the buoyancy torque which drives the vorticity is orthogonal to the induced motions (w). For the present problem, however, the basic flow induced at large N is two-dimensional, and the condition $\boldsymbol{u}$ orthogonal to $\boldsymbol{\nabla}\times\boldsymbol{u}$ is expected intuitively although the vertical variability of the horizontal motion field does give rise to some horizontal vorticity aligned with $\boldsymbol{u}_\perp$.

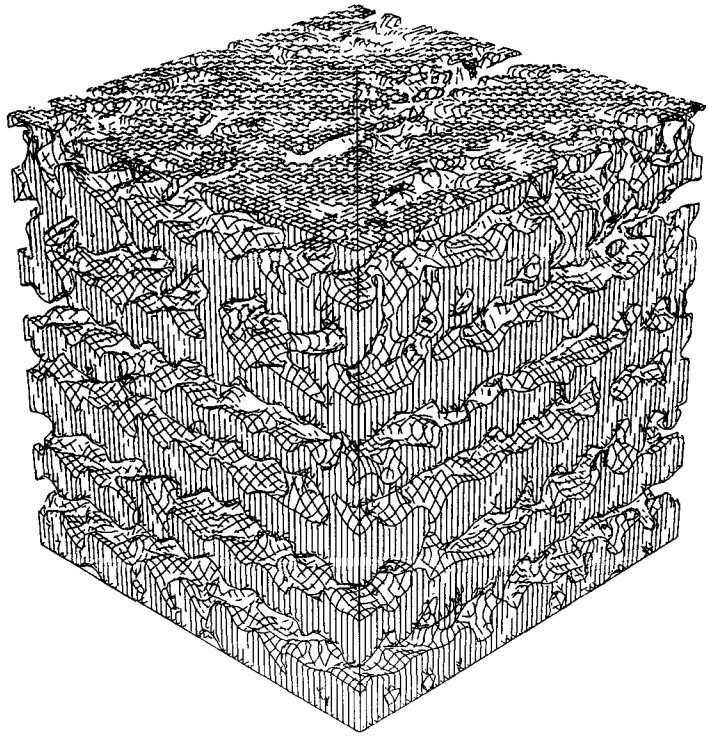

FIGURE 10. Isosurfaces of $u(x, y, z, t)$ (x-component of $\boldsymbol{u}$), during stationary phase of the flow, for $N = 80\pi$.

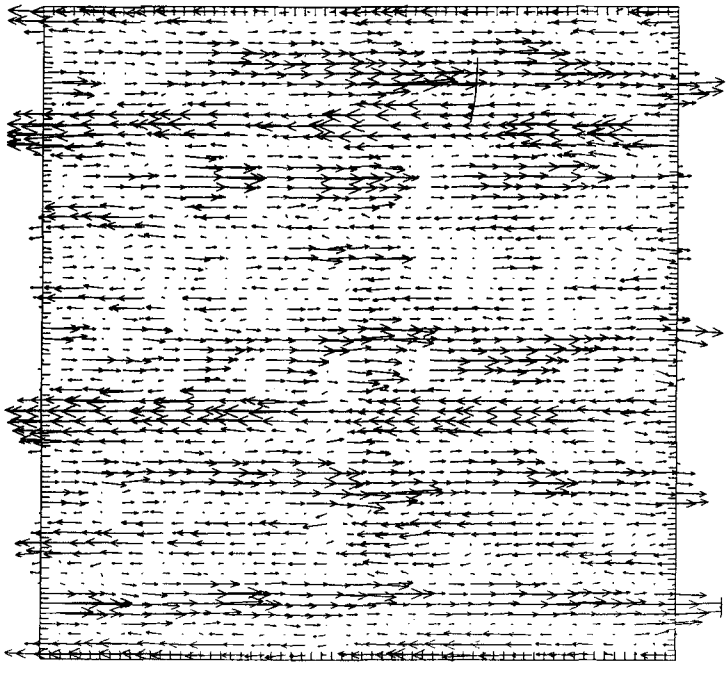

FIGURE 11. Vector plots of $\boldsymbol{u}(x, y, z, t)$, $N = 80\pi$ for (x, z)-slice at the midplanes of the flow. Flow is statistically stationary.

2.3. *Spatial structure of the flow*

Figure 10 shows isosurfaces of the horizontal motion field, $u(x, y, z, t)$, during the fully developed state of the turbulence, for $N = 80\pi$. We note complicated three-dimensional wave-like features despite the relative smallness of the vertical velocity field. The fact that this flow consists of six layers (as noted in our discussion of the k_z spectra) is clearly visible. This observation is reinforced in figure 11, which shows a vector plot of $\boldsymbol{u}$ for a vertical slice of the flow. The dominance of the horizontal motion is clear; it is, in fact, very nearly rectilinear. For $N = 20\pi$, the flow is more nearly three-dimensionally isotropic.

3. Conclusion and interpretation of results

We have described here a sequence of randomly forced, homogeneous flows, of progressively increasing (stable) stratification. If N is large enough to stabilize the flow, a further increase of N increases the two-dimensionality of the flow. But such a flow is in horizontal layers, whose thickness is set by the condition that the dissipation of kinetic energy input to the flow be attributable to the dissipation caused by the vertical variability of the horizontal flow. The condition for the onset of a stable layered-flow regime seems to be that the local Richardson number – based on the r.m.s. $\partial u/\partial z$ – be larger than unity. This stabilizes the flow against both shear and buoyant overturning (Smith, Frittz & Van Zandt 1986). The wave component of the flow becomes progressively attenuated, with amplitude $\sim N^{-1}$. Its spectrum is quite flat and tails off only because of dissipative effects, suggesting sharp wave fronts. Our results on this point are similar to the findings of Farge & Sadourny (1989) for two-dimensional shallow water waves. The amplitude of the wave component is consistent with the simple estimates of §2. The above conclusions are – of course – based on the assumptions (see, e.g. §1) that the large-t behaviour of the stratified flow (with forcing) recorded here is asymptotic.

The initial conditions of the numerical experiments consist of a two-dimensionally forced flow, upon which a small random temperature perturbation is introduced. The perturbations so introduced initially grew exponentially and were quantitatively consistent with the ($N = 0$) two-point-closure analysis (Schumann & Herring 1976). A surprising feature of these experiments is that the growth rates were independent of N. It may be that the linear phase of this problem can be understood as an instability of near-static two-dimensional vortices. Recently, Pierrehumbert (1986) and Bayly (1986) considered the stability of an isolated, elliptical vortex. They found a universal instability, whose growth rate is approximately linear in the ellipticity and proportional to the (constant) core vorticity. The connection of their analysis with the present numerical analysis is made tenuous by the time-dependence of the randomly forced field, and by the presence of a multi-vortex field with their associated distribution of ellipticities. We have examined horizontal slices of the w-field to see if the characteristic flow patterns discussed by Pierrehumbert were present, but with inconclusive results. Another work bearing on the present is that of Yakhot & Pelz (1986), who examine the stability of forced, two-dimensional flow against long-wave secondary instability. It may well be that such an instability also participates in the eventual transfer of energy to large scales for the present problem; however, Yakhot & Pelz consider special forcing functions (the so-called ABC-forcer and a purely vertical forcing function). This again makes comparisons difficult.

Our results indicate a degree of inverse cascade to large scales, but not yet a $k^{-\frac{5}{3}}$

range (the numerical results are more like $k^{-\frac{1}{2}}$). We note an appreciable accumulation of energy near the forcing wavenumber, and an associated wave–vortex interaction transferring (two-dimensional) energy into waves. Thus the two-dimensional forcing used here invokes a three-dimensionality (in the neighbourhood of the forcing function) through the instability discussed in the previous paragraph. This is in spite of the fact that the stratification is so strong that the Ozmidov wavenumber, $k_{\mathrm{O}} \equiv (N^3/\epsilon)^{\frac{1}{2}}$ is larger than the high-wavenumber cut-off ($k_{\mathrm{H}} = 32$, $k_{\mathrm{O}} \approx 80$ for $N = 80\pi$). In the neighbourhood of the forcing (perhaps a factor of 10 is the scale on either side of the forcing wavenumber, if turbulence theory is any guide) we expect ideas of inverse cascade to be vitiated. For this reason, it may be that higher resolution will allow a potential $k^{-\frac{5}{3}}$ range to emerge. On the other hand, it may be that a more judiciously chosen forcing function (one that does not excite so strongly the gravity-wave component near k_{f}) would be more conducive to inverse cascade.

We have suggested that the dissipation for large N is attributable to an equivalent friction between the layers, as observed in figures 10 and 11. This implies that the dynamics of the large-scale range is not purely inertial, but contains an appreciable frictional component. We may verify via turbulence theory, as decribed in Lesieur & Herring (1985) that such friction will indeed lessen the slope in the 'inverse-cascade' range, and steepen it in the enstrophy-cascade range.

Concerning the issue of the necessary numerical conditions for inverse cascade, we should sound a word of caution. Our computations here are 64^3 in resolution, strongly forced, with a rather large hyperviscosity ($\gamma = 16$) needed to attenuate spectra at large k. They are in addition pseudospectral. Under these conditions, the resolution may not be sufficient to examine, quantitatively, issues of inverse cascade. For example J. C. McWilliams (private communication) finds (for two-dimensional turbulence) little evidence for inverse cascade with the collocation method (pseudo-spectral) even if there is no high-wavenumber accumulation in the spectra. He observes that only if he employs the Galerkin method is inverse cascade restored. This information adds to the reasons for increased resolution.

We have also examined, briefly, certain distribution functions for the flow, in particular that for vertical shear, and the helicity density. For large Ri (small N) the distribution function for shear has a significant exponential tail, as has been observed in another context (Anselmet *et al.* 1984; McWilliams 1989). This is an interesting yet unresolved generic aspect of turbulent flows. For small Ri (large N), i.e. those calculations having significant inverse cascade; see e.g. figure 8) a surprisingly small amount of shear occurs above N. This is consistent with the fact, discussed above, that dissipation is attributable to vertical shear, almost exclusively. It should be noted that the dissipation range found here for large N is strongly anisotropic. The helicity distribution suggested that, for stratified turbulence, regions of high helicity were not as significant as for other homogeneous flows previously investigated. Our results are, in this respect, similar to those of Rogers & Moin (1986), who find that the presence of a mean strain (or shear) reduces the importance of helicity behaviour (see their figures 5 and 7) from a modest favouring of helical structures for homogeneous flows to a preference for $\boldsymbol{u} \perp (\boldsymbol{u} \times \boldsymbol{\nabla u})$. However, we have not investigated at all here the issue of whether a helical 'burst' of short duration may play a significant role in the energy transfer of stratified turbulence.

We are grateful to K. S. Gage, J. C. McWilliams, and J. J. Riley for many enlightening discussions. The basic numerical code was written by S. A. Orszag, and we are grateful to him for advice and discussions on implementing the code. S.

Jackson and B. Stankov were of considerable assistance in the early stages of programming development. The major portion of these computations were carried out at the Pittsburgh Supercomputer Center, with preliminary runs at the Boeing Supercomputer Center. Computing resources were supplied by a grant from the OASC of the National Science Foundation. NCAR is sponsored by the National Science Foundation.

REFERENCES

ANSELMET, F., GAGNE, Y. HOPFINGER, E. J. & ANTONIA, R. A. 1984 High-order velocity structure functions in turbulent shear flows. *J. Fluid Mech.* **140**, 63–89.

BAYLY, B. J. 1986 Three-dimensional instability of elliptical flow. *Phys. Rev. Lett.* **57**, 2160–2163

CHARNEY, J. G. 1971 Geostrophic turbulence. *J. Atmos. Sci.* **28**, 1087–1200.

CRAYA, A. 1958 *Contribution à l'Analyse de la Turbulence Associèe à des Vitesse Mohennes.* Publ. Sci. Tech., Ministère de l'Air (Fr), 345 pp.

CURRY, J. H., HERRING, J. R., LONCARIC, J. & ORSZAG, S. A. 1984 Order and disorder in two- and three-dimensional Bénard convection. *J. Fluid Mech.* **147**, 1–38.

FARGE, M. & SADOURNY, R. 1989 Inertial–gravity wave effects on a decaying two-dimensional turbulence in rotation. *J. Fluid Mech.* (submitted).

FERNANDO, H. J. S. 1988 The growth of a turbulent patch is stratified flow. *J. Fluid Mech.* **190**, 55–70.

GAGE, K. S. 1979 Evidence for a $k^{-\frac{5}{3}}$ law inertial range in mesoscale two-dimensional turbulence. *J. Atmos. Sci.* **36**, 1950–1954.

GAGE, K. S. & NASTROM, G. D. 1986 Theoretical interpretation of atmospheric spectra of wind and temperature observed by commercial aircraft during GASP. *J. Atmos. Sci.* **47**, 729–740.

GARRETT, C. & MUNK, W. 1979 Internal waves in the ocean. *Ann. Rev. Fluid Mech.* **11**, 339–369.

HERRING, J. R. 1974 Approach of axisymmetric turbulence to isotropy. *Phys. Fluids* **17**, 859–872.

KERR, R. M. 1987 Histograms of helicity and skewness in numerical turbulence. *Phys. Rev. Lett.* **59**, 783.

KRAICHNAN, R. H. 1967 Inertial range in two-dimensional turbulence. *Phys. Fluids* **10**, 1417–1423.

LESIEUR, M. & HERRING, J. R. 1985 Diffusion of a passive scalar in two-dimensional turbulence. *J. Fluid Mech.* **161**, 77–95.

LEVICH, E. & TSINOBER, A. 1983 On the role of helical structures in three-dimensional turbulent flows. *Phys. Lett.* **93A**, 293–297.

LILLY, D. K. 1983 Stratified turbulence and the mesoscale variability of the atmosphere. *J. Atmos. Sci.* **40**, 749–761.

MCWILLIAMS, J. C. 1989 Statistical properties of decaying geostrophic turbulence. *J. Fluid Mech.* **198**, 199–230.

ORSZAG, S. S. & PATTERSON, G. S. 1972 Numerical simulation of turbulence. In *Statistical Models and Turbulence* (ed. M. Rosenblatt and C. Van Atta). Lecture Notes in Physics, Vol. 12, pp. 127–147. Springer.

OZMIDOV, R. V. 1965 On the turbulent exchange in a stably stratified ocean. *Bull. Acad. Sci. USSR Atmos. Ocean Phys.* **1**, 493–497.

PELZ, R., SHTILMAN, L. & TSINOBER, A. 1986 The helical nature of unforced turbulent flows. *Phys. Fluids* **29**, 3506–3508.

PIERREHUMBERT, R. T. 1986 Universal short-wave instability of two-dimensional eddies in an inviscid flow. *Phys. Rev. Lett.* **57**, 2157–2159.

RILEY, J. J., METCALFE, R. W. & WEISSMAN, M. A. 1981 Direct numerical simulations of homogeneous turbulence in density stratified fluids. *Proc. AIP Conf. Nonlinear Properties of Internal Waves* (ed. B. J. West), pp. 79–112.

ROGERS, M. M. & MOIN, P. 1986 Helicity fluctuations in incompressible turbulent flows. *Phys Fluids* **30**, 2662–2671.

SCHUMANN, U. & HERRING, J. R. 1976 Axisymmetric homogeneous turbulence: a comparison of direct spectral simulations with the direct-interaction approximation. *J. Fluid Mech.* **76**, 755–782.

SMITH, S. A., FRITTZ, D. C. & VAN ZANDT, T. E. 1986 Evidence for a saturation spectrum of atmospheric gravity waves. *J. Atmos. Sci.* **44**, 1404–1410.

VAN ZANDT, T. E. 1982 A universal spectrum of buoyancy waves in the (1982) atmosphere. *Geophys. Res. Lett.* **9**, 575–578.

YAKHOT, V. & PELZ, R. 1987 Large-scale structure generation by anisotropic small-scale flows. *Phys. Fluids* **30**, 1272–1277.